temperature-dependent critical nucleation of the stable state in the metastable phase, as well as the effect of the quantum nucleation or tunneling that will give rise to temperature-independent transition probability at temperatures near zero (*11*). As seen in the inset in Fig. 3, however, the lower critical magnetic field (H_{cl}) for the metal-to-insulator transition appears to show no sign of saturation down to 1.5 K, indicating that a negligible contribution is made by the quantum tunneling process in the temperature range investigated here. The experimental data for H_{cl} can be approximately scaled with an empirical function $(H_{cl} - H_{cl}^{(0)}) \propto T^{\alpha}$, where the critical exponent α was estimated to be in the range of ¼ to ⅓, depending on the choice of $H_{cl}^{(0)}$. A solid line in the inset represents the case in which $\alpha = 4/15$.

Finally, we demonstrate the occurrence of reentrant metal-to-insulator transitions as a consequence of the peculiar electronic phase diagram of Fig. 3. Figure 4 exemplifies the resistivity change in a course of scans within the temperature field plane as shown in the inset: First, the crystal of $Nd_{1/2}Sr_{1/2}MnO_3$ was cooled from 300 K down to 4.2 K under a field of 7.5 T (route I), and then the magnetic field was decreased down to 4 T while the temperature was kept at 4.2 K. Then the crystal was warmed up to 300 K (route II) and cooled again down to 4.2 K (route III), while the field was maintained at 4 T. Corresponding to such a trajectory in the electronic phase diagram (inset, Fig. 4), the resistivity shows an irreversible behavior. In route I, the resistivity is metallic over the whole temperature range, due to the complete melting of the charge-ordered state down to 0 K, as expected from the phase diagram. The resistivity in route II shows a characteristic reentrant behavior, that is, a sequential metal-insulator-metal transition, corresponding to the traverse of the charge-ordered insulating state as temperature increased from the supercooled state at 4.2 K along route II. In this field (4 T) however, the supercooled metallic state is metastable and hence cannot be realized in such a field-cooling scan as that of route III, where only the metal-to-insulator transition is observed around 115 K. Thus the electronic (and perhaps magnetic as well as lattice-structural) properties of this compound are remarkably route dependent because of the hysteretic nature of this first-order phase transition.

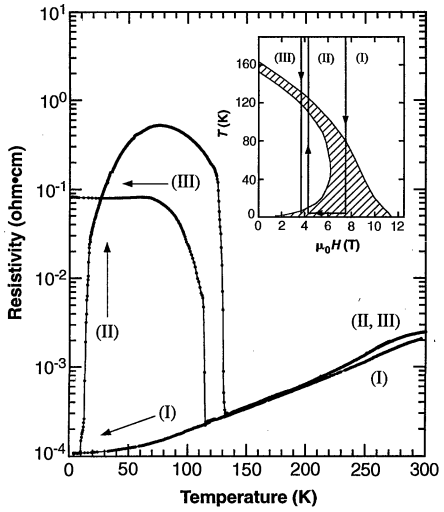

Fig. 4. Irreversible reentrant behaviors of resistivity in the crystal of $Nd_{1/2}Sr_{1/2}MnO_3$ under magnetic fields. The inset shows the trajectory of the scans of the temperature and magnetic field on the electronic phase diagram. The difference in the resistivity for routes I and II, III around $T_c = 255$ K is due to the conventional magnetoresistance (*3*) arising from the difference of the field strength (4 T and 7.5 T).

REFERENCES AND NOTES

1. J. S. Langer, *Ann. Phys.* **41**, 108 (1967); E. M. Lifshiz and L. P. Pitaevskii, in *Physical Kinetics*, vol. 10 of *Course of Theoretical Physics*, L. D. Landau and E. M. Lifshitz, Eds. (Pergamon, Oxford, 1981), pp. 427–447; J. D. Gunton, M. San Miguel, P. S. Sahni, in *Phase Transitions and Critical Phenomena*, C. Domb and J. L. Lebowitz, Eds. (Academic Press, London, 1983), vol. 8, chap. 3; C. N. R. Rao and K. J. Rao, *Phase Transitions in Solids* (McGraw-Hill, New York, 1987); J. Feder and D. S. McLachlan, *Phys. Rev.* **177**, 763 (1969).
2. G. H. Jonker and J. H. Van Santen, *Physica* **16**, 337 (1950).
3. For an example of the recent studies, see Y. Tokura *et al.*, *J. Phys. Soc. Jpn.* **63**, 3931 (1994).
4. P. W. Anderson and H. Hasegawa, *Phys. Rev.* **100**, 675 (1955); P.-G. de Gennes, *ibid.* **118**, 141 (1960).
5. K. Knízek, Z. Jirák, E. Pollert, F. Zounová, S. Vratislav, *J. Solid State Chem.* **100**, 292 (1992).
6. Y. Tomioka, A. Asamitsu, Y. Moritomo, H. Kuwahara, Y. Tokura, *Phys. Rev. Lett.* **74**, 5108 (1995).
7. C. H. Chen, S.-W. Cheong, A. S. Cooper, *ibid.* **71**, 2461 (1993).
8. Y. Moritomo, Y. Tomioka, A. Asamitsu, Y. Tokura, Y. Matsui, *Phys. Rev. B* **51**, 3297 (1995).
9. P. D. Battle, T. C. Gibb, P. Lightfoot, *J. Solid State Chem.* **84**, 271 (1990).
10. E. O. Wollan and W. C. Koehler, *Phys. Rev.* **100**, 545 (1955).
11. R. F. Voss and R. A. Webb, *Phys. Rev. Lett.* **47**, 265 (1981).
12. V. A. Bokov, N. A. Grigoryan, M. F. Bryzhina, V. V. Tikhonov, *Phys. Status Solidi* **28**, 835 (1968).

13. We thank H. Fukuyama and N. Nagaosa for enlightening discussions. Supported by the New Energy and Industrial Technology Development Organization of Japan.

19 June 1995; accepted 30 August 1995

Chemical Generation of Acoustic Waves: A Giant Photoacoustic Effect

Huxiong Chen and Gerald Diebold

An anomalous photoacoustic effect is produced when a suspension of carbon particles in water is irradiated by a high-power, pulsed laser. The photoacoustic effect has an amplitude on the order of 2000 times that produced by a dye solution with an equivalent absorption coefficient and gives a distinctly audible sound above an uncovered cell. Transient grating experiments with carbon suspensions show a doubling of the acoustic frequency corresponding to the optical fringe spacing of the grating. The effect is thought to originate in high-temperature chemical reactions between the surface carbon and the surrounding water.

The photoacoustic effect (*1*–*8*) takes place when radiation is absorbed by a body: the thermal expansion of the body that occurs when optical radiation is converted to heat causes mechanical motion of the body, which, in turn, launches a sound wave into the surrounding medium. In this report, we describe an anomalously large photoacoustic effect in aqueous suspensions of fine carbon particles. We used a conventional photoacoustic apparatus together with a pulsed laser to compare the amplitude of the effect in carbon suspensions with that produced by an absorbing dye solution. Suspensions of carbon (30 nm in diameter) were made by the addition of dry carbon black (9) to distilled water in a standard spectrophotometer cuvette at a concentration of 55 mg liter^{-1}. The suspensions were sonicated in an ultrasonic cleaning bath for 30 s until the carbon was uniformly dispersed in the water.

In preliminary experiments, the photoacoustic effect displayed an induction period where the magnitude of the acoustic signal gradually increased as the suspension was irradiated by the laser. The cuvette was therefore first irradiated with the 15-ns, 532-nm output of a *Q*-switched Nd:yttrium-aluminum-garnet laser for 3000 shots, with the laser operating at 160 mJ per shot. Then a small sample of the irradiated suspension was withdrawn from the cuvette, diluted with distilled water, and placed in a photoacoustic cell equipped with a polyvinyl-

Department of Chemistry, Brown University, Providence, RI 02912, USA.

idene fluoride (PVDF) film transducer, whose output was displayed on a fast oscilloscope. The laser beam was directed into the cell through Pyrex windows in a cylindrical excitation geometry, with the propagation direction of the laser beam parallel to the face of the transducer.

If the sound production results from thermal expansion of the irradiated fluid, the magnitude of the photoacoustic signal in the weak absorption limit is directly proportional to the optical absorption coefficient $\bar{\alpha}$ of the fluid, as is well known from theory and experiments with dye solutions (*5*, *10*–*12*). We thus compared the signals from carbon suspensions with those from nonfluorescent aqueous dye solutions, taking the ratio of the photoacoustic signal amplitude to the optical absorption coefficient as the basis for comparison. (The dye used here, malachite green, has a lifetime in solution that is significantly shorter than the 15-ns-long pulse width of the laser.) Optical absorption coefficients of undiluted carbon suspensions and malachite green solutions in distilled water were measured with a conventional spectrophotometer. The experiments showed (*13*) that the carbon suspensions, when scaled to their optical absorption coefficients in the photoacoustic cell, gave acoustic signals that were as much as 2000 times larger than those for the dye solutions.

Even dilute carbon suspensions (for example, 10 mg liter^{-1}) when irradiated with a 1 cm in diameter, 100-mJ laser beam, gave a distinctly audible cracking noise that could be heard from the open end of the cell on each firing of the laser. The acoustic signal emitted into the air surrounding the photoacoustic cell grew steadily in amplitude as the laser was repeatedly fired, reaching a maximum typically after about 3000 shots, coincident with the maximum in the signal amplitude detected in solution with the PVDF transducer. Electron micrographs showed that before irradiation, the samples contained agglomerated groups (9) of carbon spheres 30 nm in diameter. The first effect of irradiation was to produce new particles with a shell-like structure whose diameters ranged from 30 to 400 nm; with prolonged irradiation, the concentration of large particles increased at the expense of the original particles. The production of large-diameter particles was accompanied by a gradual loss of total carbon in the suspension, as evidenced by a decrease in optical absorbance on irradiation, until the suspension became transparent. The formation of precipitates or other solid reaction products was not indicated by the spectrophotometric measurements.

Ultrasonic waves were excited in the suspensions by first splitting the laser beam and then recombining the two beams in a geometry that produces an optical standing wave. Absorption of the optical radiation at the antinodes of the electric field produces impulsive temperature and pressure increases in the fluid, which launch high-frequency acoustic standing waves. Because acoustic waves have time-dependent density variations, a probe laser beam directed at the Bragg angle to the propagation direction of the acoustic wave is diffracted. The diffracted beam intensity is proportional to the square of the density variation in the sound wave. This method, whereby a grating is produced by two laser beams and its time evolution is monitored by a probe beam at the Bragg angle, is referred to as the "transient grating" technique (*14*, *15*), also known by the acronyms "LIPS" (*16*) or "ISTS" (*17*). A continuous He-Ne probe laser was used together with a fast digitizing oscilloscope to record the intensity of the diffracted light signal. We used an aqueous gold sol (*18*), which has a strong plasmon absorption at 532 nm, as a control. The experimental waveform from the gold sol (Fig. 1A) can be explained by a simple thermal expansion model for acoustic wave production and is typical of signals that are commonly produced by a variety of short-lifetime dyes in solution (*15*, *16*, *19*).

The transient grating signal from a carbon suspension (Fig. 1B) has a component not only at the fundamental frequency corresponding to the optical fringe spacing but also at the first overtone. The overtone was found to have an induction period as well. As the suspension was first irradiated, a weak signal at the fundamental frequency was seen. On further irradiation, the diffracted light signal increased in intensity, with the magnitude of the overtone growing to nearly that of the fundamental. Gradually, over the course of a few thousand laser shots (at the radiation intensity level and carbon concentrations listed in the caption to Fig. 1), the fundamental and overtone signals disappeared together as the solution became transparent.

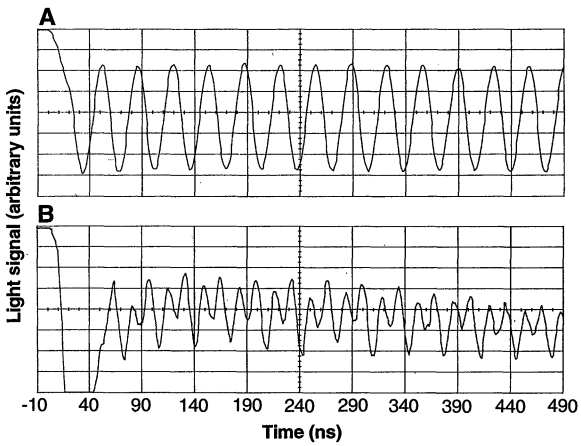

Fig. 1. (**A**) Plot of the diffracted light signal versus time for a gold sol showing the initiation of a 28.8-MHz standing acoustic wave. The frequency of the sound wave corresponds to the frequency for a grating with a fringe spacing of 50 μm. (**B**) Corresponding plot of the diffracted light signal versus time for a carbon suspension. The signal was taken after irradiation of the solution with 3000 firings of the laser at 100 mJ per shot. In addition to the normal frequency component of the wave at 28.8 MHz, the wave train shows a strong component of the first overtone. Both the gold and carbon samples were irradiated by a laser beam 1 cm in diameter in a 1 cm by 1 cm by 4 cm magnetically stirred cuvette. For both traces, the baseline is the top line of the graticule; the oscilloscope was triggered 10 ns before the firing of the laser. Both traces show scattered light reaching the detector at the beginning of the trace. The laser pulse energy was 160 mJ in (A) and 100 mJ in (B). The signal in (A) is an average over 32 shots; (B) is a single-shot recording.

The photoacoustic effect is generally attributed to thermal expansion of the irradiated fluid. Because the thermal expansion coefficient of water is nearly linearly dependent on temperature and vanishes at 4°C, we measured the magnitude of the transient grating signal as a function of temperature to delineate the importance of thermal expansion as the mechanism of sound production. Cooling the cuvette from room temperature to a few degrees Celsius resulted in greatly reduced transient grating signals: no diffracted light signal could be detected in the range of 1° to 4°C. Surprisingly though, amplitude measurements of the ultrasonic wave produced in the cylindrical excitation geometry with the PVDF transducer showed no decrease over the same temperature range. The amplitude of the sharp noise generated above the suspension (measured with a conventional electret microphone) similarly showed no decrease over the same temperature range.

The gradual reduction in the absorbance of the suspensions recorded in the transient grating experiments suggests that the particles are heated sufficiently to cause chemical reactions between the carbon particles and the surrounding water: when a glass U-tube filled with a carbon suspension was irradiated, several cubic centimeters of stable gases collected above the liquid. A gas chromatographic analysis of the trapped gases (using a Spherocarb column with thermal conductivity detection) indicated the presence of H_2 and CO, as would be produced by the well-known, endothermic steam-carbon reaction (*20*).

A model to describe the photoacoustic effect that includes chemical reaction must include the consumption or liberation of thermal energy and volume changes produced on the conversion of reactants to products. In the case of the steam-carbon reaction, the volume change is substantial because of the great disparity between the molar volume of gases such as H_2 and CO and liquid water. Consideration of the effects of energy consumption and volume change in the linearized hydrodynamic equations for a fluid (*21*) gives the acoustic density δ and temperature τ as solutions to the coupled equations

$$\left(\nabla^2 - \frac{\gamma}{c^2}\frac{\partial^2}{\partial t^2}\right)\delta = -\rho\beta\,\nabla^2\tau - \rho\beta_c\nabla^2 n \quad (1)$$

and

$$\lambda\,\nabla^2\tau - \rho C_V\frac{\partial\tau}{\partial t} = -H + \rho\mu^\dagger\frac{\partial n}{\partial t} - \frac{C_V(\gamma - 1)}{\beta}\frac{\partial\delta}{\partial t} \quad (2)$$

where γ is the heat capacity ratio, c is the speed of sound, t is time, ρ is the ambient density, β is the thermal expansion coefficient, β_c is a "chemical" expansion coefficient, n is the differential concentration of new chemical species formed, λ is the thermal conductivity, C_V is the heat capacity at constant volume, H is the "heating function" (the energy per volume and time delivered to the fluid by the light beam), and $\mu^\dagger$ is a chemical potential. The chemical expansion coefficient is a measure of the change in fluid density at constant pressure P and temperature T on conversion of reactants to products, defined by

$$\beta_c = -\frac{1}{\rho}\left(\frac{\partial\rho}{\partial N}\right)_{P,T} \quad (3)$$

where N is the concentration of chemical species reacted. The chemical potential is the amount of internal energy per mass stored per concentration of chemical species reacted at constant density and temperature and is defined as

$$\mu^\dagger = \left(\frac{\partial\epsilon}{\partial N}\right)_{\rho,T} \quad (4)$$

where ϵ is the internal energy per mass of the fluid.

Equation 1 is essentially a wave equation for the acoustic density, and Eq. 2 is a heat equation for the temperature change coupled through a compressive work term, the $\partial\delta/\partial t$ term in Eq. 2. The two source terms on the right side of Eq. 1 show that changes in either the temperature or the chemical composition act identically to launch acoustic waves. The term in Eq. 2 containing the chemical potential acts as an energy source, or sink, that augments or diminishes H. A solution to Eqs. 1 and 2 for a transient grating problem, with the heat deposition taken as rapid compared with the acoustic period, and the evolution of chemical species taken to be of the form $n = n_0[1 - \exp(-t/\tau)]$, where n_0 is the concentration of new chemical species produced, gives the acoustic density as a sum over three terms (*22*),

$$\delta(\hat{t}) = \frac{\bar{\alpha}\beta E_0}{C_P}[\hat{\delta}_1(\hat{t}) + \hat{\delta}_2(\hat{t}) + \hat{\delta}_3(\hat{t})]\cos kx \quad (5)$$

where $\bar{\alpha}$ is the optical absorption coefficient of the fluid, E_0 is the energy per area in the laser beam, C_P is the heat capacity at constant pressure, k is the grating wave vector, and x is the distance along the grating. The three density contributions are given by

$$\hat{\delta}_1(\hat{t}) = \left(1 - \frac{\zeta}{1 - \hat{\ell}_h\hat{\tau}}\right)(-e^{-\hat{\ell}_h\hat{t}} + \cos\hat{t}) \quad (6)$$

$$\hat{\delta}_2(\hat{t}) = \zeta\left(\frac{1}{1 - \hat{\ell}_h\hat{\tau}} - \frac{C_P\beta_c}{\tilde{h}\beta}\right) \times \left[\frac{-e^{-\hat{t}/\hat{\tau}} + \cos\hat{t} - \left(\frac{1}{\hat{\tau}}\right)\sin\hat{t}}{1 + \left(\frac{1}{\hat{\tau}}\right)^2}\right] \quad (7)$$

$$\hat{\delta}_3(\hat{t}) = \zeta\left(\frac{C_P\beta_c}{\tilde{h}\beta}\right)(-1 + \cos\hat{t}) \quad (8)$$

where $\hat{t}$ is a dimensionless time defined as $\hat{t} = ckt$, $\hat{\tau}$ is a dimensionless rise time defined as $\hat{\tau} = ck\tau$, $\hat{\ell}_h$ is a dimensionless heat conduction length defined as $\hat{\ell}_h = \lambda k/\rho C_P c$, ζ is the fraction of the deposited optical energy converted into chemical energy defined as $\zeta = \rho\tilde{h}n_0/\bar{\alpha}E_0$, and $\tilde{h}$ is the change in enthalpy per mass of the fluid per change in the concentration of reactants given by $\tilde{h} = (\partial h/\partial N)_{P,T}$ where h is the enthalpy per mass of the fluid.

The $\hat{\delta}_1$ term in Eq. 5 for typical values of $\hat{\ell}_h$ in fluids describes a slowly decaying exponential wave and a sinusoidal wave, commonly referred to (*21*) as the "thermal" and "acoustic" modes of wave motion, respectively. The acoustic mode describes nearly adiabatic waves that arise from the rapid temperature and pressure jumps following heat deposition at the antinodes of the optical beam, whereas the thermal mode describes the changes in state variables resulting from the deposition of heat at the antinodes and their slow decay through conduction of heat into the nodal regions of the fluid. On the time scale of the wave shown in Fig. 1A, the thermal and acoustic modes balance each other; on squaring the density, only the fundamental frequency corresponding to the optical fringe spacing appears in the diffracted light signal. The effect of chemical reactions, described by the $\hat{\delta}_2$ term, is to alter only the overall amplitude of the signal. The $\hat{\delta}_3$ term in the expression for the acoustic density depends only on the volume change produced by the chemical reaction. As in the case of the $\hat{\delta}_1$ term, there is no imbalance in the amplitudes of the two terms. The $\hat{\delta}_2$ term in Eq. 5, on the other hand, can become purely sinusoidal if the time scale for chemical reaction is fast enough for the exponential decay term to vanish, leaving only the sinusoidal terms. If the density is described by an expression where the sinusoidal component is larger than an exponentially decaying component, then the diffracted light signal, proportional to the square of the acoustic density, will contain an overtone of the fundamental frequency.

For a given quantity of energy, the gas volume produced by the carbon-steam reaction is approximately 8000 times what would be produced by thermal expansion of water at room temperature; that is, the prefactor of the $\hat{\delta}_3$ term is over three orders of magnitude larger than unity. However, the theory given above does not take into account either the time for accumulation of dissolved gas to form a bubble or the low acoustic impedance of a gas relative to that of water, the latter governing the rate at which a gas can expand against a dense fluid. It is thus possible that, on a time scale of a few hundred nanoseconds, thermal expansion is more important than chemical expansion in the production of acoustic waves, so that only $\hat{\delta}_1$ (Eq. 6) and first term in $\hat{\delta}_2$ (Eq. 7) are important in a description of the grating. A purely thermal mechanism for generation of the grating signal is indicated by its disappearance near 4°C. This interpretation is further supported by the appearance of an overtone in the diffracted light signal, which requires not only the dominance of a thermal mechanism but also a fast decay of the exponential term in $\hat{\delta}_2$. In fact, for the laser pulse width and the optical fringe spacing in the transient grating experiments here, $1/\hat{\tau}$ is approximately 5; a rapid decay of the exponential term and a significant contribution of the first term in $\hat{\delta}_2$ to the total acoustic density are thus expected.

The time scale for the photoacoustic effect in the cylindrical excitation geometry is given by the diameter of the laser beam divided by the sound speed. For the experiments here, this figure is 7 μs, which is large compared with the time scale for the transient grating experiments. Audible signals correspond to even longer time scales. Thus, a slow but substantial gas expansion whose development time is governed by the low acoustic impedance of the gas could

account for the large magnitude of the acoustic signal seen in the cylindrical excitation geometry, the audible sound, and the failure of both of these signals to disappear at low temperature. The reaction of carbon with water takes place at temperatures on the order of hundreds of degrees Celsius; thus, the production and expansion of gas should be essentially independent of temperature for a change as small as 10°C. The induction period for the photoacoustic effect in carbon suspensions can, in all likelihood, be ascribed either to the increased reactivity of the new, large-diameter particles that are formed during irradiation or to the development of reaction centers in the graphitic component of the carbon, as has been noted for the steam-carbon reaction (*23*).

The theory given here for chemical generation of the photoacoustic effect should be rigorously correct for differential changes in the state variables. However, its application to the present rather complicated problem, where high-temperature reactions and gas expansion are involved, is speculative. In addition to chemical reaction, phenomena such as temperature-dependent thermal expansion (*1*, *5*, *24*), nonlinear heat conduction (*25*), vaporization of fluid around the perimeter of the particle (*20*), and even shock-wave formation are possibly involved in the generation of the photoacoustic effect. The unusual properties of the photoacoustic effect in carbon suspensions, its ease of production (*26*), and its dependence on chemical reaction argue for more experimentation and, most certainly, for formulation of a more sophisticated theoretical model for sound wave generation.

REFERENCES AND NOTES

1. V. E. Gusev and A. A. Karabutov, *Lazernaya Optoakustika* (Naoka, Moscow, 1991) [transl., *Laser Optoacoustics* (AIP Press, New York, 1993)].
2. F. V. Bunkin, Al A. Kolomensky, V. G. Mikhalevich, *Lasers in Acoustics* (Harwood Academic, Reading, MA, 1991).
3. S. V. Egerev, L. M. Lyamshev, O. V. Puchenkov, *Usp. Fiz. Nauk* **160**, 111 (1990) [*Sov. Phys. Usp.* **33**, 739 (1990)].
4. S. A. Akhmanov, V. E. Gusev, A. A. Karabutov, *Infrared Phys.* **29**, 815 (1989).
5. A. C. Tam, *Rev. Mod. Phys.* **58**, 381 (1986).
6. A. I. Bozhkov, F. V. Bunkin, Al. A. Kolomenskii, V. G. Mikhalevich, *Sov. Sci. Rev.* **3**, 459 (1981).
7. C. K. N. Patel and A. C. Tam, *Rev. Mod. Phys.* **53**, 517 (1981).
8. L. M. Lyamshev, *Usp. Fiz. Nauk* **135**, 637 (1981) [*Sov. Phys. Usp.* **24**, 977 (1981)].
9. Experiments were done with "Black Pearls 470" (Cabot Inc.). The diameters of the individual particles were determined from electron micrographs to be on the order of 30 nm. The agglomeration seen on the micrographs was consistent with the 94-nm hydrodynamic diameter specified by the manufacturer.
10. G. J. Diebold, M. I. Khan, S. M. Park, *Science* **250**, 101 (1990).
11. M. I. Khan, T. Sun, G. J. Diebold, *J. Acoust. Soc. Am.* **94**, 931 (1993).
12. G. J. Diebold, T. Sun, M. I. Khan, *Phys. Rev. Lett.* **67**, 3384 (1991).
13. A number of experiments were done with different carbon and dye solutions. The suspension with the largest normalized experiment had an undiluted absorption coefficient of $\bar{\alpha} = 0.092\ cm^{-1}$. This solution was diluted by a factor of 500 in the photoacoustic cell and gave a photoacoustic signal of 150 mV. The malachite green dye solution used for comparison had $\bar{\alpha} = 0.07\ cm^{-1}$ and gave a photoacoustic signal of 20 mV.
14. H. J. Eichler, P. Gunter, D. W. Pohl, *Laser-Induced Dynamic Gratings* (Springer-Verlag, Berlin, 1985).
15. R. J. D. Miller, in *Time Resolved Spectroscopy*, R. J. H. Clark and R. E. Hester, Eds. (Wiley, New York, 1989), pp. 1–54.
16. M. D. Fayer, *IEEE J. Quantum Electron.* **QE-22**, 1437 (1986).
17. A. R. Duggal and K. A. Nelson, *J. Chem. Phys.* **94**, 7677 (1991).
18. Purchased from Ted Pella, Inc. The diameter of the gold particles is specified to be 40 nm with a standard deviation of ±10 nm, at a concentration of 5.8×10^{-2} g liter^{-1} or 9×10^{10} particles per milliliter.
19. J. Morais, J. Ma, M. B. Zimmt, *J. Phys. Chem.* **95**, 3885 (1991).
20. The production of gas is corroborated by the work of K. J. McEwan and P. A. Madden [*J. Chem. Phys.* **97**, 8748 (1992)], who inferred the production of bubbles around the particles by carrying out experiments with pressurized carbon suspensions. H. Lowne and P. A. Madden [*J. Chem. Phys.* **97**, 8760 (1992)] gave a model for sound production based on fluid vaporization.
21. P. Morse and K. U. Ingard, *Theoretical Acoustics* (Princeton Univ. Press, Princeton, NJ, 1968).
22. The chemical expansion coefficient β_c given here should be the molar volume change determined experimentally by a number of organic photochemists and discussed by S. E. Braslavsky and H. E. Heibel [*Chem. Rev.* **92**, 1381 (1992)]; both have the same dimensions. Note that Eq. 5 has been calculated to zeroth order in ℓ_h in the acoustic mode. The effects of viscosity have not been included in the abbreviated solution given here. For a complete solution, see H. Chen and G. Diebold (in preparation).
23. C. G. von Fredersdorff and M. A. Elliott, in *The Chemistry of Coal Utilization*, Supplementary Volume, H. H. Lowry, Ed. (Wiley, New York, 1963), pp. 918–925. In the limit where the particle diameter is much smaller than the wavelength of the optical radiation, it is easy to show that the final temperature of a particle is independent of its radius if there are no thermal loss mechanisms. When heat is lost from a particle by thermal conduction, calculations show that large particles remain at an elevated temperature longer than small ones, indicating a higher effective reactivity for large particles.
24. M. W. Sigrist, *J. Appl. Phys.* **60**, R83 (1986).
25. V. Gusev, A. Mandelis, R. Bleiss, *Int. J. Thermophys.* **14**, 321 (1993).
26. A. Harata and T. Sawada (in preparation) have found large signals and nonlinear effects from carbon suspensions in experiments with surface waves on fluids.

27. This research was supported by the U.S. Department of Energy, Office of Basic Energy Studies, under grant ER-13235.

26 May 1995; accepted 12 September 1995

Supramolecular Second-Order Nonlinearity of Polymers with Orientationally Correlated Chromophores

Martti Kauranen, Thierry Verbiest, Carlo Boutton, M. N. Teerenstra, Koen Clays, A. J. Schouten, R. J. M. Nolte, André Persoons*

Nonlinear optical chromophores can be organized as orientationally correlated side groups of polymers with a rigid backbone. In such an organization, each chromophore contributes coherently to the second-order nonlinear response of the polymer structure. A first hyperpolarizability exceeding 5000×10^{-30} electrostatic units was measured for a poly(isocyanide) structure containing ~100 chromophores by means of hyper-Rayleigh scattering. Electric field–induced second-harmonic generation measurements confirmed that the product of the permanent dipole moment and the first hyperpolarizability was enhanced for the polymer structure. These results provide guidelines for future efforts to optimize supramolecular structures for applications in second-order nonlinear optics.

Organic molecules are widely regarded as one of the most promising groups of materials for applications in nonlinear optics (*1*). For several important applications, such as electro-optic modulation or frequency doubling, materials with second-order nonlinearity are required. Only noncentrosymmetric molecules (or aggregates) can possess a second-order nonlinear response, that is, a nonvanishing first molecular hyperpolarizability. Moreover, the molecules cannot be useful in devices unless they are incorporated into a noncentrosymmetric macroscopic structure, which has a nonvanishing second-order susceptibility. The achievement of such macroscopic ordering is a formidable task, because the permanent dipole moments of noncentrosymmetric molecules tend to pair in opposite directions to give rise to a centrosymmetric macroscopic structure.

The most common way to break the

M. Kauranen, T. Verbiest, C. Boutton, K. Clays, A. Persoons, Laboratory of Chemical and Biological Dynamics and Center for Research on Molecular Electronics and Photonics, University of Leuven, B-3001 Heverlee, Belgium.

M. N. Teerenstra and A. J. Schouten, Laboratory of Polymer Science, University of Groningen, 9747 AG Groningen, Netherlands.

R. J. M. Nolte, Department of Organic Chemistry, University of Nijmegen, 6525 ED Nijmegen, Netherlands.

*To whom correspondence should be addressed.